Hindawi Publishing Corporation
Journal of Nanomaterials
Volume 2015, Article ID 346238, 7 pages
http://dx.doi.org/10.1155/2015/346238

Research Article

Improvement of the Magnetic Properties of Nanocrystalline $Nd_{12.3}(FeZrNbCu)_{81.7}B_{6.0}$ Alloys with Dy Substitutions

Weiwei Yang,[1] Leichen Guo,[2] Zhimeng Guo,[1] Guangle Dong,[3] Yanli Sui,[3] and Zhian Chen[4]

[1]*School of Materials Science and Engineering, University of Science and Technology Beijing, Beijing 100083, China*
[2]*School of Engineering, Rensselaer Polytechnic Institute, NY 12180-3590, USA*
[3]*State Key Laboratory for Advanced Metals and Materials, University of Science and Technology Beijing, Beijing 100083, China*
[4]*Beijing Zhong Ke San Huan Hi-Tech Co., Ltd, Beijing 100090, China*

Correspondence should be addressed to Zhimeng Guo; guozhimengustb@163.com

Received 21 December 2014; Accepted 4 January 2015

Academic Editor: Christian Brosseau

$Nd_{12.3-x}Dy_xFe_{81.7}Zr_{0.8}Nb_{0.8}Cu_{0.4}B_{6.0}$ (x = 0–2.5) ribbons have been prepared by melt-spun at 30 m/s and subsequent annealing. The influence of addition of Dy on the crystallization behavior, magnetic properties, and microstructure were investigated. Differential scanning calorimeter (DSC) and X-ray diffraction (XRD) revealed a single-phase material. Microstructure studies using transmission electron microscopy (TEM) had shown a significant microstructure refinement with Dy addition. Wohlfarth's analysis showed that the exchange coupling interactions increased first with Dy content x increasing, reached the maximum value at x = 0.5, and then slightly decreased with x further increasing. Optimal magnetic properties with J_r = 1.09 T, H_{ci} = 1048 kA/m, and $(BH)_{max}$ = 169.5 kJ/m^3 are achieved by annealing the melt-spun ribbons with x = 0.5 at% at 700°C for 10 min.

1. Introduction

Nd-Fe-B magnets markets have been growing [1] and nanocrystalline Nd-Fe-B has been developed as an essential permanent magnet material for industrial applications [2]. The nanostructure and the composition of the alloy have an influence on the magnetic properties of the isotropic nanocrystalline Nd-Fe-B permanent magnets; extensive efforts have been made via some special methods [3, 4] or adjusting composition to improve the magnetic properties. At present, elemental substitution has been found to be one of the most effective methods for excellent performance. Pr, Zr, Nb, Cu, and Dy substitutions have been widely used in Nd-Fe-B magnets. Studies indicate that Zr or Nd addition can inhibit grain growth, leading to much finer microstructure and higher magnetic properties [5–7]. Cu and Nb addition also can extend the temperature range of the heat-treatment for optimizing the magnetic properties [8]. As we know that the magnetocrystalline anisotropy field (H_A) of $Dy_2Fe_{14}B$ (H_A = 12576.8 kA/m) is much higher than the one of $Nd_2Fe_{14}B$ (H_A = 5572 kA/m) [9], Dy substitutes Nd can improve the magnetocrystalline anisotropy field (H_A) and optimize the microstructure of the $Nd_2Fe_{14}B$ matrix and decrease the grain size [10]. The researchers in the past have been concentrating on nanocomposite $Fe_3B/Nd_2Fe_{14}B$ or $Nd_2Fe_{14}B/\alpha$-Fe [11, 12]. However, the report of the single addition of Dy was rare. In this work, we present our research about the crystallization behavior, microstructure, magnetic properties, and exchange coupling of single phase $Nd_{12.3-x}Dy_xFe_{79.7}Zr_{0.8}Nb_{0.8}Cu_{0.4}B_{6.0}$ (x = 0–2.5) ribbons.

2. Experiment

The $Nd_{12.3-x}Dy_xFe_{79.7}Zr_{0.8}Nb_{0.8}Cu_{0.4}B_{6.0}$ (x = 0–2.5) ribbons were obtained by applying the melt-spinning technique at a wheel speed of 30 m/s. The ribbon samples with a width of 2-3 mm and a thickness of 40–50 μm were isothermally annealed at 600–800°C for 10 min in vacuum-sealed quartz tubes to crystallize. Phase analysis of the samples was characterized by X-ray diffractometer with Cu-Kα radiation. The crystallization behavior was examined by differential scanning calorimetry (DSC). Magnetic measurement at room

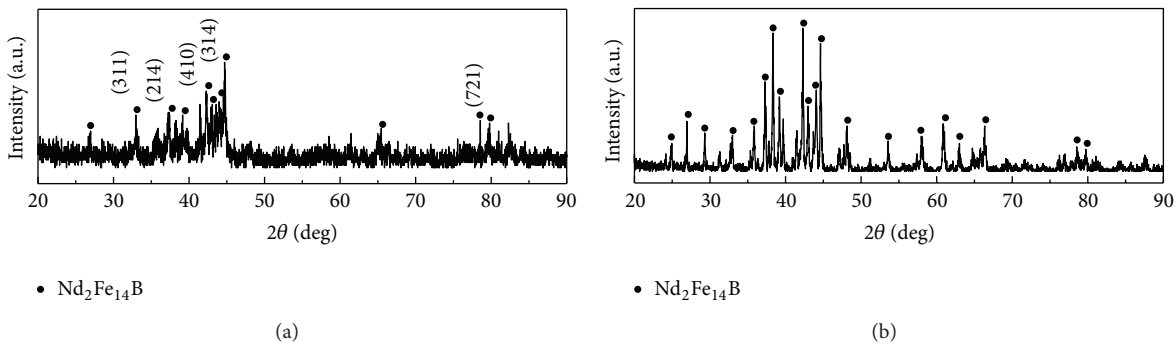

FIGURE 1: XRD patterns of $Nd_{10.8}Dy_{1.5}Fe_{79.7}Zr_{0.8}Nb_{0.8}Cu_{0.4}B_{6.0}$. (a) Melt-spun ribbon at a speed of 30 m/s; (b) as-cast alloy annealed at 1050°C for 10 h.

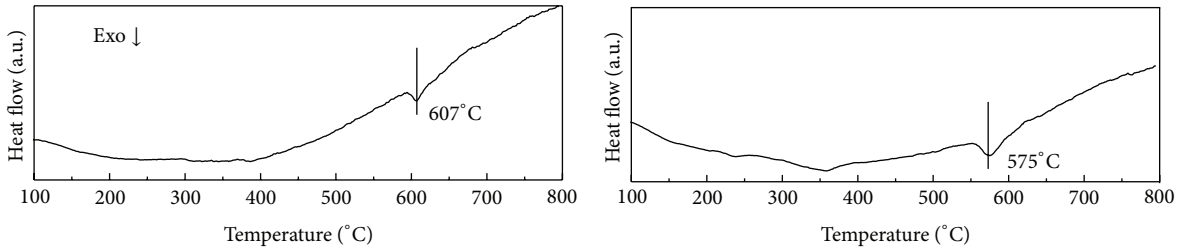

FIGURE 2: DSC curves for melt-spun ribbons with different Dy content. (a) $Nd_{10.8}Dy_{1.5}Fe_{79.7}Zr_{0.8}Nb_{0.8}Cu_{0.4}B_{6.0}$; (b) $Nd_{12.3}Fe_{81.7}B_{6.0}$.

temperature was employed using a LDJ9600 vibrating sample magnetometer (VSM). The length direction of the ribbons was parallel to the applied field in order to minimize demagnetization effect. The microstructures were observed by high-resolution transmission electron microscopy (HR-TEM JEM2010) with thin foils prepared by ion-beam thinning.

3. Results and Discussion

3.1. Phase Analysis. Figure 1 shows the XRD patterns of $Nd_{10.8}Dy_{1.5}Fe_{79.7}Zr_{0.8}$-$Nb_{0.8}Cu_{0.4}B_{6.0}$ at different condition. Figure 1(a) shows the alloy has partial crystallization and highlights the weak characteristic peaks of $Nd_2Fe_{14}B$. This indicates that those ribbons still have many amorphous phases and the grain size of the crystalline phase is small. Figure 1(b) shows XRD pattern of as-cast $Nd_{10.8}Dy_{1.5}Fe_{79.7}Zr_{0.8}Nb_{0.8}Cu_{0.4}B_{6.0}$ alloy annealed at 1050°C for 10 h. The only crystalline phase in the matrix is 2 : 14 : 1 phase at both the annealed condition and as-spun condition. After the annealing treatment, the $Nd_2Fe_{14}B$ grains were completely formed, and there is no new phase appearing in the grain boundary. This result provides the possibility of the magnetic exchange coupling interaction between the adjacent grains.

Figure 2 shows the differential scanning calorimetry (DSC) curves of the as-spun ribbons with different Dy content at a heating rate of 10°C/min from room temperature to 800°C and the thermal properties determined from these DSC thermal scans are summarized in Table 1. Samples with $x = 1.5$ at% and without other elements of $Nd_{12.3}Fe_{81.7}B_{6.0}$ show one exothermic peak corresponding to the transformation from amorphous phase to 2 : 14 : 1 phase. It is in accordance with the XRD result in Figure 1. Compared with the curve of $Nd_{12.3}Fe_{81.7}B_{6.0}$, the ribbon with substitution of 1.5 at% Table 1 and Figure 1 show that Dy and other additional elements retarded the onset temperature of crystallization and peak temperature of crystallization. When the temperature reaches 580°C, the alloy with additional elements has no crystallization. The contrary crystallization phenomenon of improving crystallization tendency of the Mn substitution in $Nd_2Fe_{14}B/\alpha$-Fe nanocomposites was also observed by Xie et al. [13].

3.2. Effect of Dy Content on Magnetic Properties of Ribbons. Since the amorphous phase is undesired, in order to achieve the best magnetic properties for the samples with different Dy content, a thermal treatment at 600–800°C for 10 min is employed individually to quenched ribbons. Figure 3 summarizes variation of H_{ci}, J_r, and $(BH)_{max}$ with Dy content. The intrinsic coercivity H_{ci} significantly increases with increasing Dy content. That is because the magnetocrystalline anisotropy field (H_A) of the $Dy_2Fe_{14}B$ (12600 kA/m) is larger than that of the $Nd_2Fe_{14}B$ (5600 kA/m) and they are totally mutual soluble [9]. The remanence J_r of Dy from 0 at% to 0.5 at% doped samples shows little change. Then, the J_r decreases with increasing Dy content. On the one hand, the saturation magnetization (J_s) of $Dy_2Fe_{14}B$ (0.71 T) is smaller than that of the $Nd_2Fe_{14}B$ (1.60 T) [14]. As we all know that Nd and Dy are both rare elements and chemical properties, the atomic radius of Dy is larger than that of Nd. When Dy atoms substitute the site of Nd atoms, the volume and the local atomic structure of Nd will be influenced. With

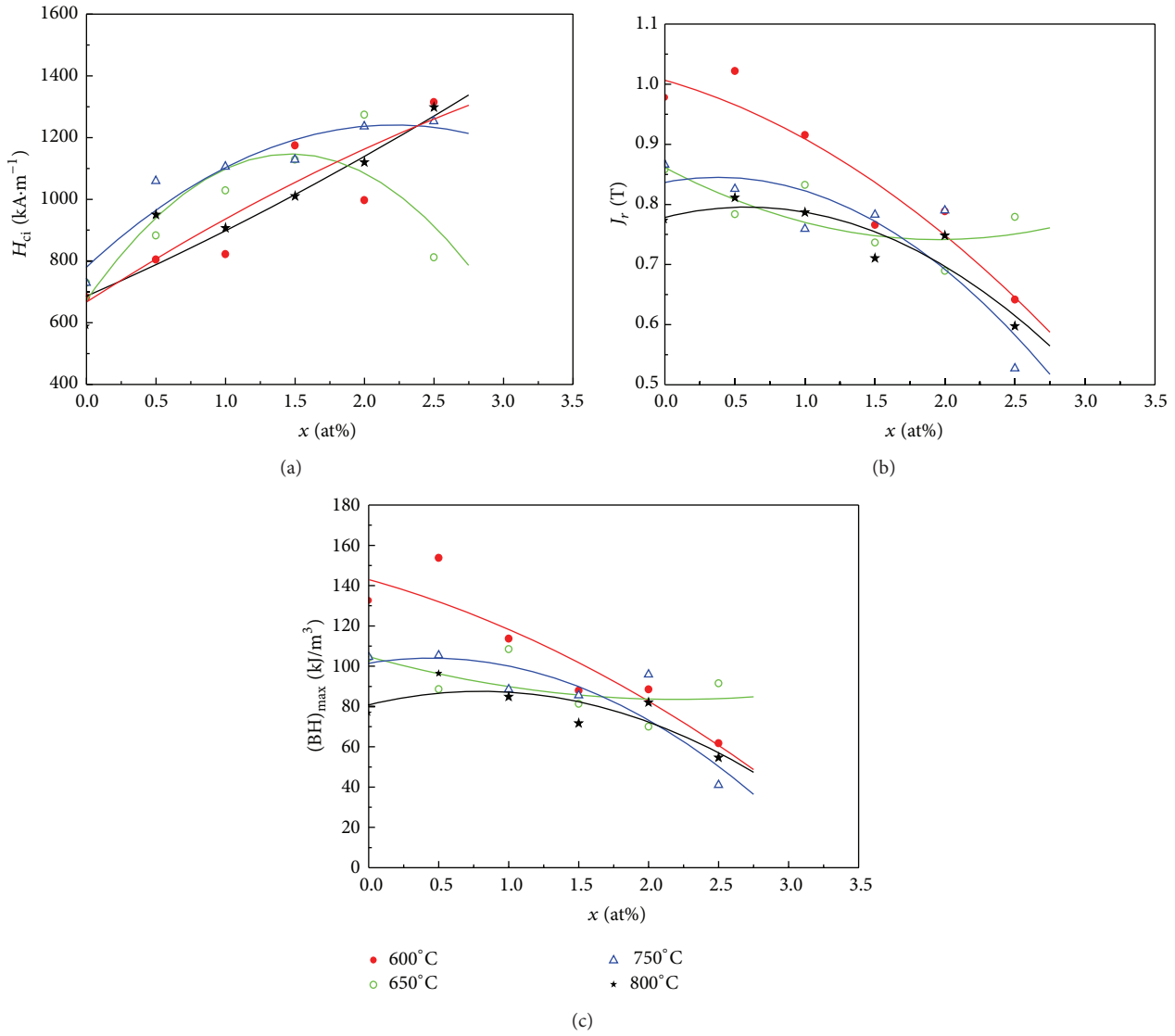

FIGURE 3: Magnetic properties of the $Nd_{12.3-x}Dy_xFe_{79.7}Zr_{0.8}Nb_{0.8}Cu_{0.4}B_{6.0}$ ribbons at various temperatures for 10 min. (a) H_{ci}; (b) J_r; (c) $(BH)_{max}$.

TABLE 1: Summary of thermal properties of the melt-spun ribbons alloys determined from the DSC curves.

	$Nd_{12.3}Fe_{81.7}B_{6.0}$	$Nd_{10.8}Dy_{1.5}Fe_{79.7}Zr_{0.8}Nb_{0.8}Cu_{0.4}B_{6.0}$	ΔT
T_x (°C)	575	607	32
T_p (°C)	562	597	35

T_x: onset temperature of crystallization; T_p: peak temperature of crystallization.

further Dy addition, the effect of Dy on reducing J_s and J_r becomes stronger and the remanence decreases. Magnetic energy product $(BH)_{max}$ increases initially and then decreases and reaches the peak value when the content of Dy is 0.5 at%. When the content of Dy is more than 1.0 at%, $(BH)_{max}$ begins to greatly reduce, due to the deviation of demagnetization curve square degree.

The optimal magnetic properties were indicated in Table 2. As can be seen, the addition of Dy can improve significantly the magnetic properties. A small amount of Dy can refine the grains and optimize the microstructure. After the optimum annealing treatment, the coercivity of $Nd_{10.8}Dy_{1.5}Fe_{79.7}Zr_{0.8}$-$Nb_{0.8}Cu_{0.4}B_{6.0}$ is enhanced from 775.5 kA/m for $x = 0$ to 1440 kA/m for $x = 2.0$. However, with the increase of the Dy content, the remanence is increased first from 0.98 T for $x = 0$ to 1.09 T $x = 0.5$ and then decreased to 0.98 T for $x = 2.0$. The maximum energy product is increased firstly and then decreased. All the maximum energy products of the annealed sample with Dy substitution are larger than 130 kJ/m^3. Optimum magnetic

Table 2: Optimal magnetic properties of $Nd_{12.3-x}Dy_xFe_{79.7}Zr_{0.8}Nb_{0.8}Cu_{0.4}B_{6.0}$ at different experiment conditions.

Dy (at%)	$(BH)_{max}$ (kJ/m^3)	H_{ci} (kA/m)	J_r (T)	J_r/J_s	Process conditions
0	132.7	750.6	0.98	0.73	600°C 10 min
0.5	168.7	1048.1	1.09	0.70	700°C 10 min
1.5	158.7	1360.9	1.05	0.74	600°C 10 min
2.0	130.8	1440.2	0.98	0.71	750°C 10 min

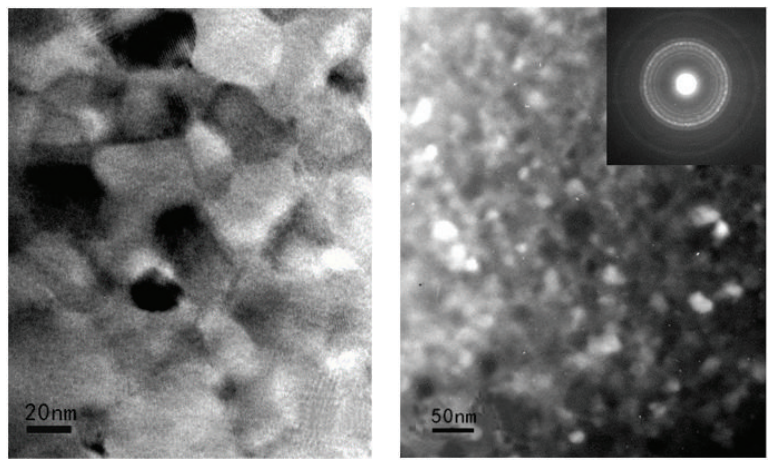

(a) (b)

Figure 4: TEM micrographs of $Nd_{12.3-x}Dy_xFe_{79.7}Zr_{0.8}Nb_{0.8}Cu_{0.4}B_{6.0}$ ribbons annealed at 700°C for 10 min: (a) $x = 0$; (b) $x = 0.5$.

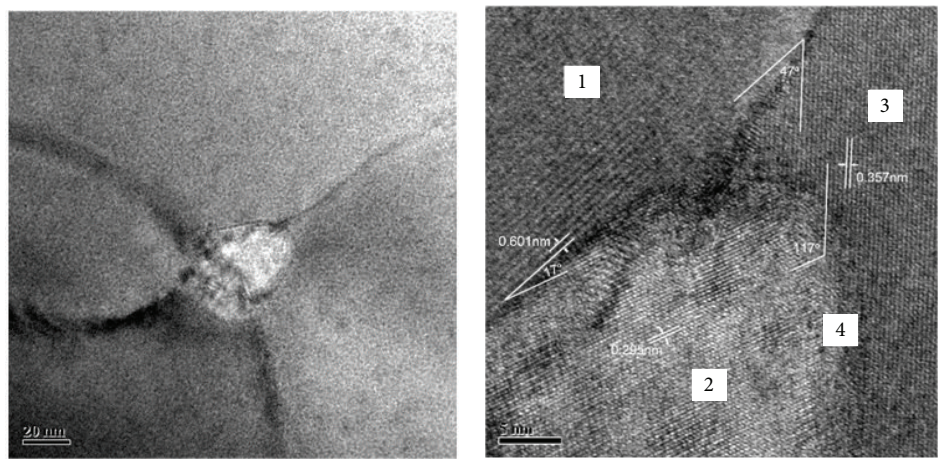

(a) (b)

Figure 5: HR-TEM images of the $Nd_{12.3-x}Dy_xFe_{79.7}Zr_{0.8}Nb_{0.8}Cu_{0.4}B_{6.0}$ ($x = 1.5$) annealed ribbon: (a) low amplification; (b) high amplification.

properties with $J_r = 1.09$ T, $H_{ci} = 1048$ kA/m and $(BH)_{max} = 169.5$ kJ/m^3 are achieved by annealing the melt-spun ribbons with $x = 0.5$ at% at 700°C for 10 min. Compared to the Dy-free sample, H_{ci}, J_r, and $(BH)_{max}$ of alloy with $x = 0.5$ at% are increased by 40%, 11%, and 27%.

3.3. Effect of Dy Content on Microstructure. Figure 4 shows TEM images of the Dy-free and Dy-containing ribbons annealed at 700°C for 10 min. The average grain size is estimated to be 40 to 60 nm for the Dy-free ribbons and the grain size of the Dy-doped ribbons is significantly finer. The average grain size for the samples with $x = 0.5$ is estimated to be 30 to 50 nm, and the grains become more uniformly distributed. It implies that the slight amount of Dy is effective to uniform the grains and suppress the growth of the grains during the heat treatment. The fine and homogeneous microstructure is favored for exchange coupling interaction.

Figure 5 shows the HR-TEM images of $Nd_{12.3-x}Dy_xFe_{79.7}Zr_{0.8}Nb_{0.8}Cu_{0.4}B_{6.0}$ annealed at 700°C for 10 min. The special morphology phase (large grains are mixed up with small grains) is 2 : 14 : 1 phase and

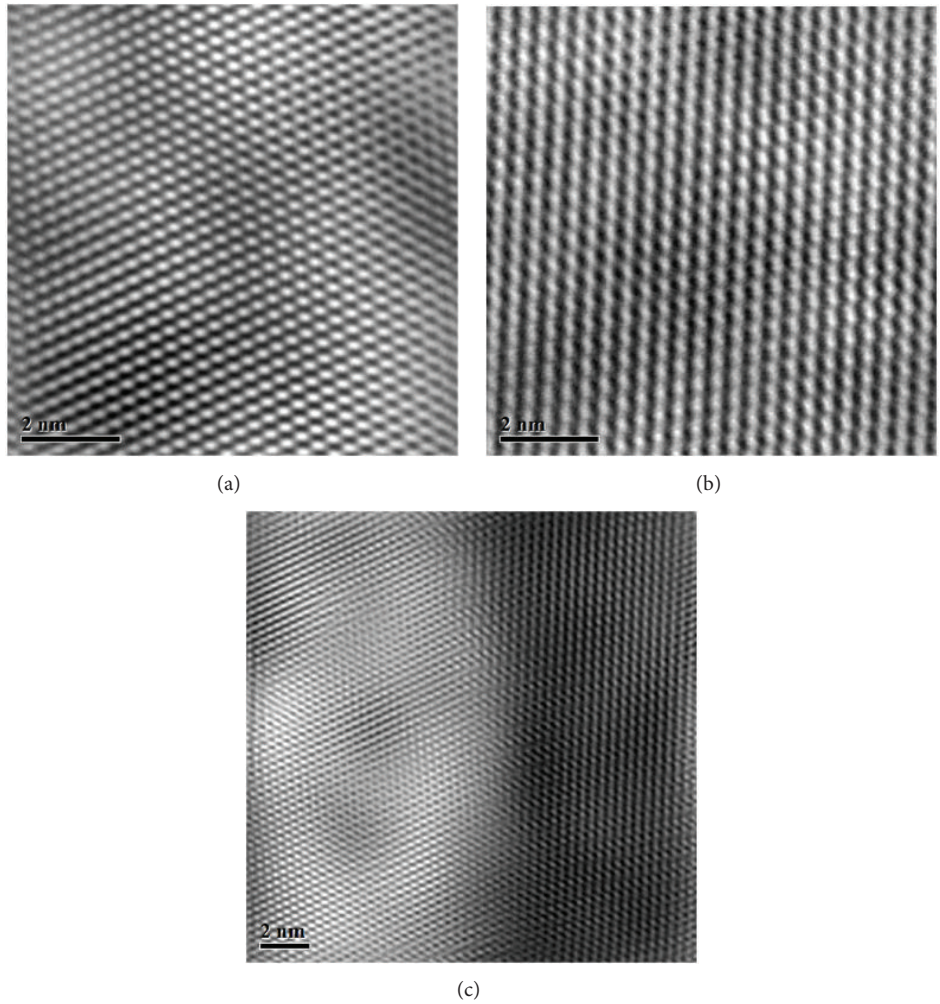

(a) (b)

(c)

FIGURE 6: Fourier filtered images corresponding to different sections in Figure 5(b). (a) Corresponding to Figure 5(b) zone 2; (b) corresponding to Figure 5(b) zone 3; (c) corresponding to Figure 5(b) zone 4.

the crystallization is perfectly complete. No boundary phase is found between the grains. The grain boundaries are totally crystallographically coherent. This is different from the structure of the sintered NdFeB magnets, whose coercivity dramatically depends on the Nd-rich phase between and around the grains. In order to further analyze the large grains sandwiched small grains inside the grains and on the grain boundaries, the Fourier filtered images corresponding to different sections of Figure 5 are shown in Figure 6. As can be seen, either inside the grains or on the grain boundaries, the lattice regular arrangement and the grain boundaries are partly coherent. No second phase or grain boundary phase is found. It also proves that the coercivity mechanism in this series of materials is not similar to the traditional one in the sintered magnets. The magnetic coercivity is probably realized by the effect of the magnetic exchange-coupling interaction between grains.

The exchange coupling interaction is often evaluated using δM plots [15], which can be defined as $\delta M(H) = m_d(H) - (1 - 2m_r(H))$, in which m_d is reduced magnetization and m_r is reduced remanence with respect to the applied magnetic field, H. According to Wohlfarth's analysis [16], higher positive $\delta M(H)$ peaks indicate stronger exchange coupling interactions among grains. Figure 7 shows plots of $\delta M(H)$ for the annealing $Nd_{12.3-x}Dy_xFe_{79.7}Zr_{0.8}Nb_{0.8}Cu_{0.4}B_{6.0}$ (x = 0–2.0) samples. All samples are composed of one magnetically hard phase, and the remanence ratio J_r/J_s is larger than 0.5, which indicates the existence of the exchange coupling between grains. It is clear that the magnitude of δM peaks increases first with Dy content increasing and reaches maximum value at $x = 0.5$ and then decreases with further increase of Dy content, indicating that the intergranular exchange coupling effect appears to strengthen with the increase of x up to 0.5 and then diminish with further increase in x. The plots of $\delta M(H)$ for $Nd_{10.3}Dy_2Fe_{79.7}Zr_{0.8}Nb_{0.8}Cu_{0.4}B_{6.0}$ (x = 2.0) sample has still a high peak. According to Wohlfarth's analysis, higher positive $\delta M(H)$ peaks indicate stronger exchange coupling interactions among grains. The XRD pattern in Figure 1(b) shows that there is only one crystalline phase ($Nd_2Fe_{14}B$). It

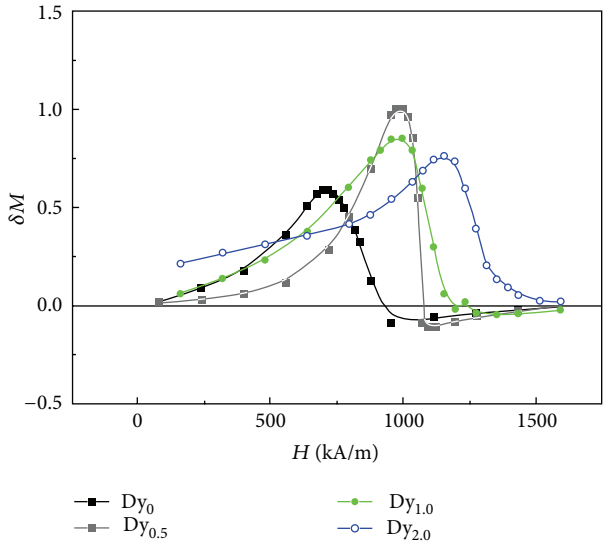

FIGURE 7: The $\delta M(H)$ cures of $Nd_{12.3-x}Dy_xFe_{79.7}Zr_{0.8}Nb_{0.8}Cu_{0.4}B_{6.0}$ (x = 0–2.0) ribbons annealed at 700°C for 10 min.

can imply that has a strong exchange coupling effect between $Nd_2Fe_{14}B$ grains. The $\delta M(H)$ cure of x = 2.0 at% has a wide curve peak in the positive axis. The trend is a change in the magnetic energy with Dy content. The exchange coupling interactions increased fist with Dy content x increasing, reached the maximum value at x = 0.5, and then slightly decreased with x further increasing. The magnetic properties and it is consistent. Hence, the changes in magnetic properties of the samples on increasing Dy content may mainly arise from the variation of the exchange coupling interaction in the samples.

4. Conclusion

Magnetic properties of nanocrystalline $Nd_{12.3}Fe_{81.7}Zr_{0.8}Nb_{0.8}Cu_{0.4}B_{6.0}$ ribbons prepared by melt spinning and subsequent annealing were significantly enhanced by the substitution of Dy for Nd. The main results obtained are the following:

(1) The slight content of Dy stabilized the amorphous phase and enhanced the thermal stability of amorphous phase in the melt-spun.

(2) The intrinsic coercivity H_{ci} and maximum energy product $(BH)_{max}$ increased with increased with increasing Dy content and then decreased with further increasing Dy content. However, the remanence polarization J_r decreased with Dy content monotonically. The excellent magnetic properties with $(BH)_{max}$ = 169.5 kJ/m^3, H_{ci} = 809.2 kA/m, and J_r = 1.02 T were obtained by annealing a melt-spun amorphous $Nd_{11.8}Dy_{0.5}Fe_{81.7}Zr_{0.8}Nb_{0.8}Cu_{0.4}B_{6.0}$ alloy at 700°C for 10 min.

(3) The exchange coupling interactions increased first with Dy content x increasing, reached the maximum value at x = 0.5, and then slightly decreased with x further increasing. In all samples, they have a strong exchange coupling between neighboring grains. The fine and homogeneous microstructure is favored for exchange coupling interaction.

Conflict of Interests

The authors declare that there is no conflict of interests regarding the publication of this paper.

Acknowledgment

This study is supported by the National Natural Science Foundation of China under Grant no. 51174030.

References

[1] L. Yang, "Development of NdFeB magnet industry in new century," *Journal of Iron and Steel Research International*, vol. 13, no. 1, pp. 1–11, 2006.

[2] O. Gutfleisch, M. A. Willard, E. Brück, C. H. Chen, S. G. Sankar, and J. P. Liu, "Magnetic materials and devices for the 21st century: stronger, lighter, and more energy efficient," *Advanced Materials*, vol. 23, no. 7, pp. 821–842, 2011.

[3] B. Z. Cui, M. Q. Huang, R. H. Yu et al., "Magnetic properties of $(Nd,Pr,Dy)_2Fe_{14}B/\alpha$-Fe nanocomposite magnets crystallized in a magnetic field," *Journal of Applied Physics*, vol. 93, no. 10, pp. 8128–8130, 2003.

[4] Z. C. Wang, S. Z. Zhou, M. C. Zhang, and Y. Qiao, "High-performance α-Fe/$Pr_2Fe_{14}B$-type nanocomposite magnets produced by hot compaction under high pressure," *Journal of Applied Physics*, vol. 88, no. 1, pp. 591–593, 2000.

[5] H. Hashino, Y. Tazaki, H. Ino, T. Ohkubo, and K. Hono, "Effects of Zr and C additions on the magnetic properties and structures of melt-spun $Fe_{83}Nd_{10}B_7$-based nanocomposite magnets," *Journal of Magnetism and Magnetic Materials*, vol. 278, no. 1-2, pp. 68–75, 2004.

[6] L. Jun, L. Ying, and M. Yilong, "Effect of niobium on microstructure and magnetic properties of bulk anisotropic NdFeB/α-Fe nanocomposites," *Journal of Magnetism and Magnetic Materials*, vol. 324, no. 14, pp. 2292–2297, 2012.

[7] H. W. Chang, Y. T. Cheng, C. W. Chang et al., "Improvement of size and magnetic properties of $Nd_{9.5}Fe_{72.5}Ti_3B_{15}$ bulk magnets by Zr or Nb substitution for Ti," *Journal of Applied Physics*, vol. 105, no. 7, Article ID 07A742, 2009.

[8] D. H. Ping, K. Hono, H. Kanekiyo, and S. Hirosawa, "Microalloying effect of Cu and Nb on the microstructure and magnetic properties of $Fe_3B/Nd_2Fe_{14}B$ nanocomposite permanent magnets," *IEEE Transactions on Magnetics*, vol. 35, no. 5, pp. 3262–3264, 1999.

[9] S. G. Kim, M. J. Kim, K. S. Ryu, Y. B. Kim, C. S. Kim, and T. K. Kim, "Effect of Dy on magnetic properties of α-Fe/$Nd_2Fe_{14}B$ type alloy," *IEEE Transactions on Magnetics*, vol. 35, no. 5, pp. 3316–3318, 1999.

[10] Z. Liu and H. A. Davies, "Elevated temperature study of nanocrystalline (Nd/Pr)–Fe–B hard magnetic alloys with Co and Dy additions," *Journal of Magnetism and Magnetic Materials*, vol. 290-291, part 2, pp. 1230–1233, 2005.

[11] W. F. Miao, J. Ding, P. G. McCormick, and R. Street, "Magnetic behaviour of mechanically milled $(Nd_{1-x}Dy_x)_8Fe_{88}B_4$," *Journal*

of Magnetism and Magnetic Materials, vol. 175, no. 3, pp. 304–310, 1997.

[12] X. Fang, Y. Shi, and D. C. Jiles, "Modeling of magnetic properties of heat treated dy-doped NdFeB particles bonded in isotropic and anisotropic arrangements," *IEEE Transactions on Magnetics*, vol. 34, no. 4, pp. 1291–1293, 1998.

[13] G. Z. Xie, J. X. Xu, P. H. Lin et al., "Magnetic properties of Mn substituted Nd–Fe–B composite," *Journal of Magnetism and Magnetic Materials*, vol. 278, no. 1-2, pp. 179–184, 2004.

[14] S. Hirosawa, Y. Matsuura, H. Yamamoto, S. Fujimura, M. Sagawa, and H. Yamauchi, "Magnetization andmagnetic anisotropy of $R_2Fe_{14}B$ measured on single crystals," *Journal of Applied Physics*, vol. 59, no. 3, pp. 873–879, 1986.

[15] P. E. Kelly, K. O'Grady, P. I. Mayo, and R. W. Chantrell, "Switching mechanisms in cobalt-phosphorus thin films," *IEEE Transactions on Magnetics*, vol. 25, no. 5, pp. 3881–3883, 1989.

[16] E. P. Wohlfarth, "Relations between different modes of acquisition of the remanent magnetization of ferromagnetic particles," *Journal of Applied Physics*, vol. 29, no. 3, pp. 595–596, 1958.